ADVANCED
FUNCTIONAL
MATERIALS

Supporting Information

for *Adv. Funct. Mater.,* DOI: 10.1002/adfm.201808117

Highly Surface-Wrinkled and N-Doped CNTs Anchored on Metal Wire: A Novel Fiber-Shaped Cathode toward High-Performance Flexible Li–CO_2 Batteries

*Yinchuan Li, Jingwen Zhou, Tingbo Zhang, Tianshuai Wang, Xuelian Li, Yafu Jia, Jianli Cheng, Qun Guan, Enzuo Liu, Huisheng Peng, and Bin Wang**

Supporting Information

Highly Surface-Wrinkled and N-Doped CNTs Anchored on Metal Wire: A Novel Fiber-Shaped Cathode toward High-Performance Flexible Li-CO_2 Batteries

*Yinchuan Li, Jingwen Zhou, Tingbo Zhang, Tianshuai Wang, Xuelian Li, Yafu Jia, Jianli Cheng, Qun Guan, Enzuo Liu, Huisheng Peng and Bin Wang**

Y. Li, J. Zhou and T. Zhang contributed equally to this work.

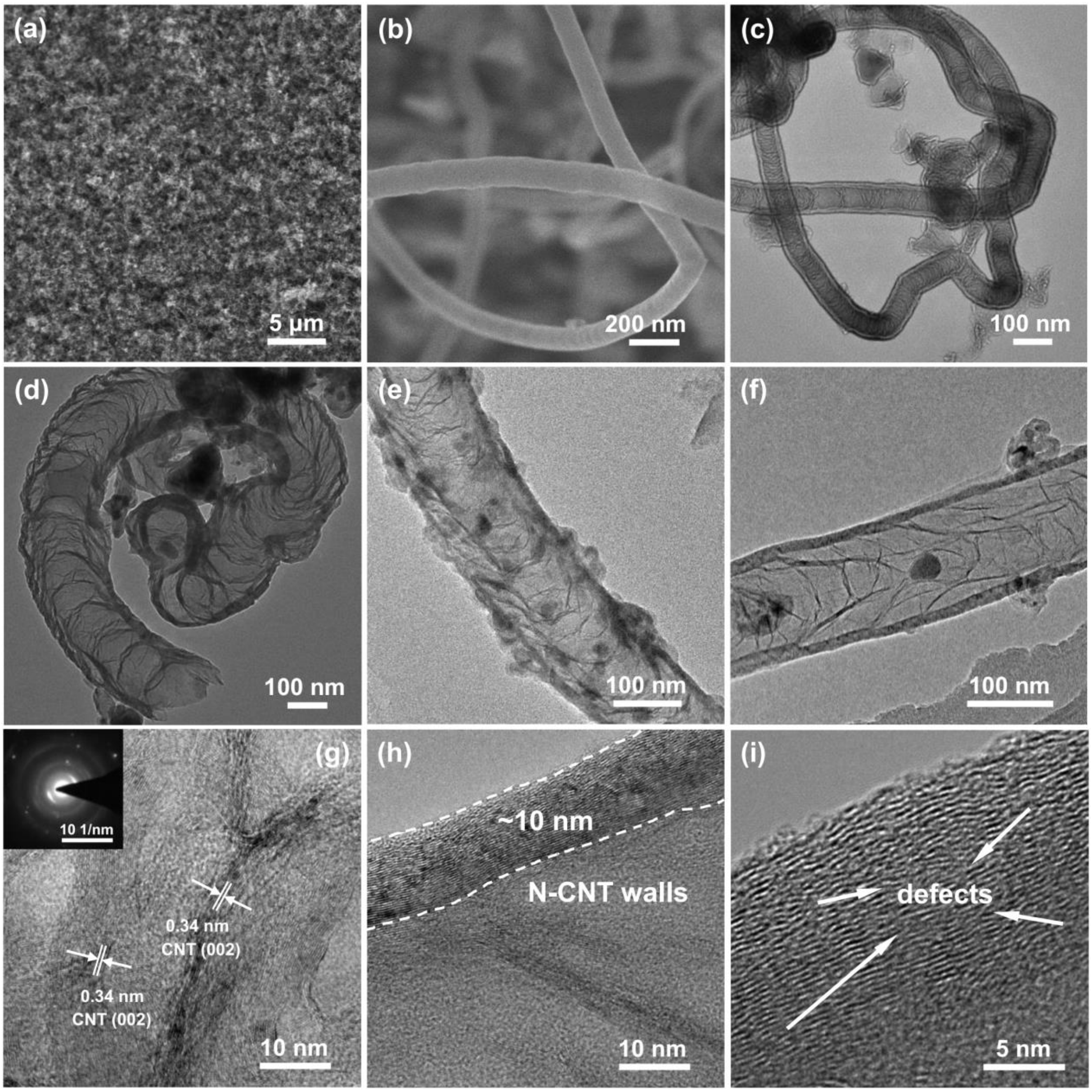

Figure S1. (a) Typical SEM, (b) FE-SEM, (c-f) TEM and (g-i) HRTEM images with a SAED pattern inset in (g) of the as-synthesized highly surface-wrinkled and N-doped CNT networks anchored on Ti wire.

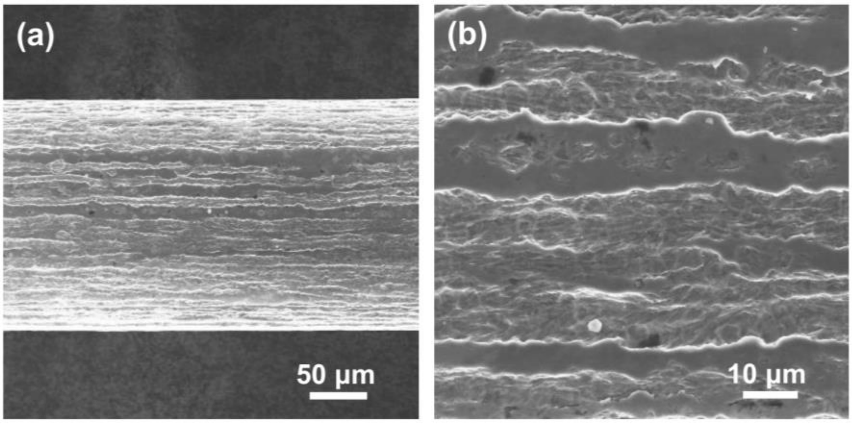

Figure S2. (a,b) Typical SEM images of the Ti wire with the diameter of 210 µm after being cleaned by acetone, alcohol and distilled water, respectively.

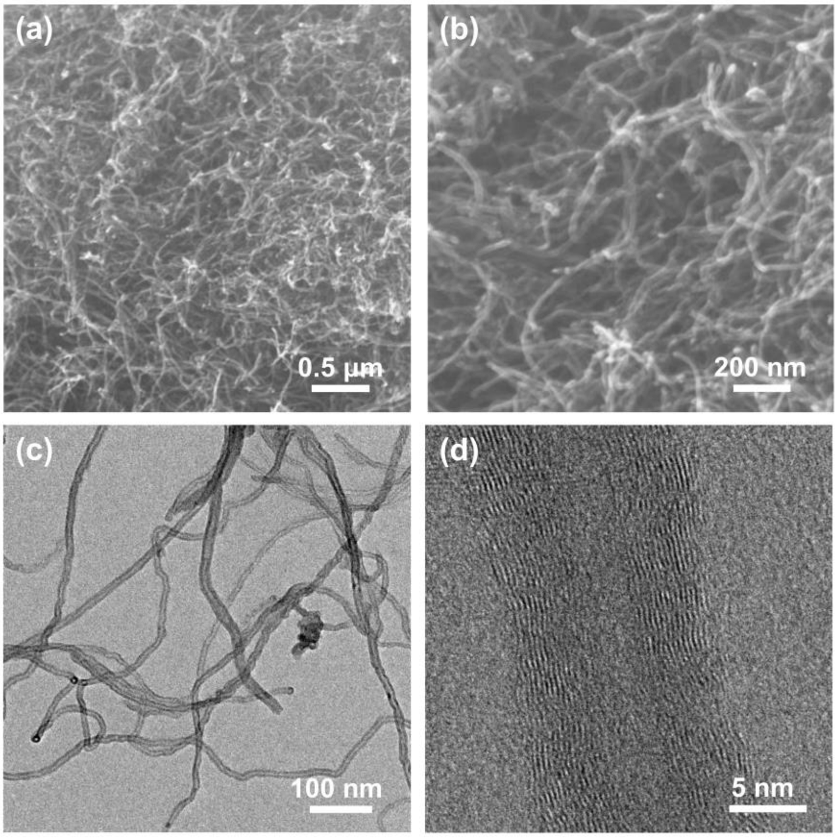

Figure S3. (a,b) SEM and (c,d) TEM images of commercial carboxylic multi-walled CNT powders (CNT-COOH) with the average diameter of 20-30 nm.

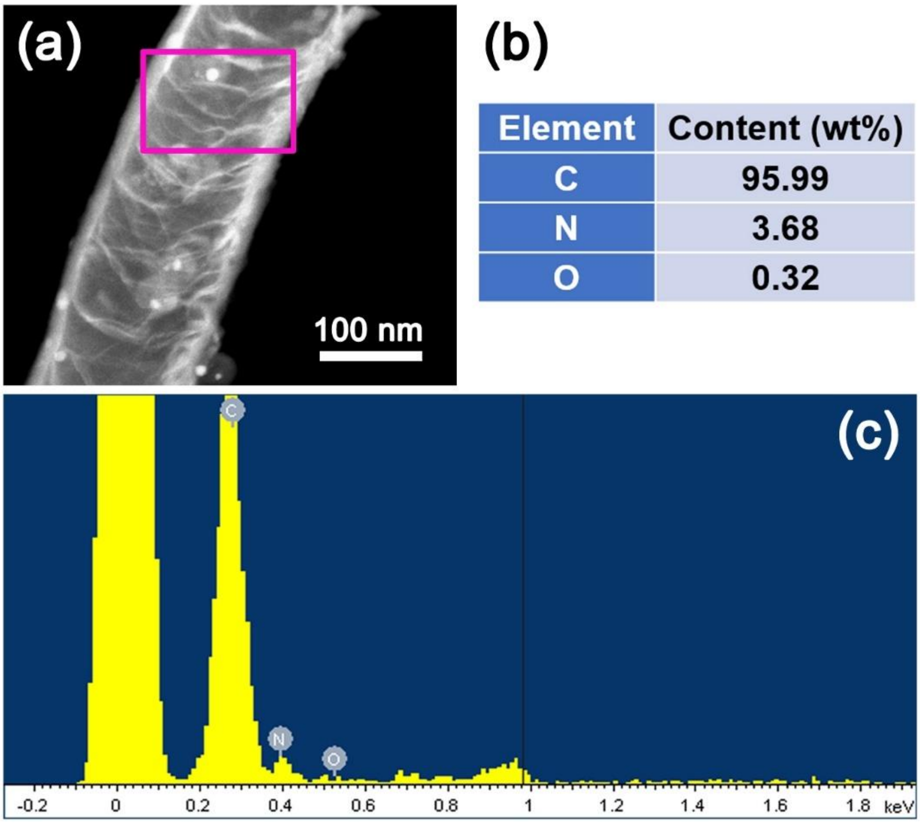

Element	Content (wt%)
C	95.99
N	3.68
O	0.32

Figure S4. (a) Dark field TEM image of an individual highly surface-wrinkled and N-doped CNT extracted from Ti wire. (b) Element content of C, N and O, and (c) EDX spectrum corresponding to the selected area (indexed by pink rectangle) of N-CNT shown in (a).

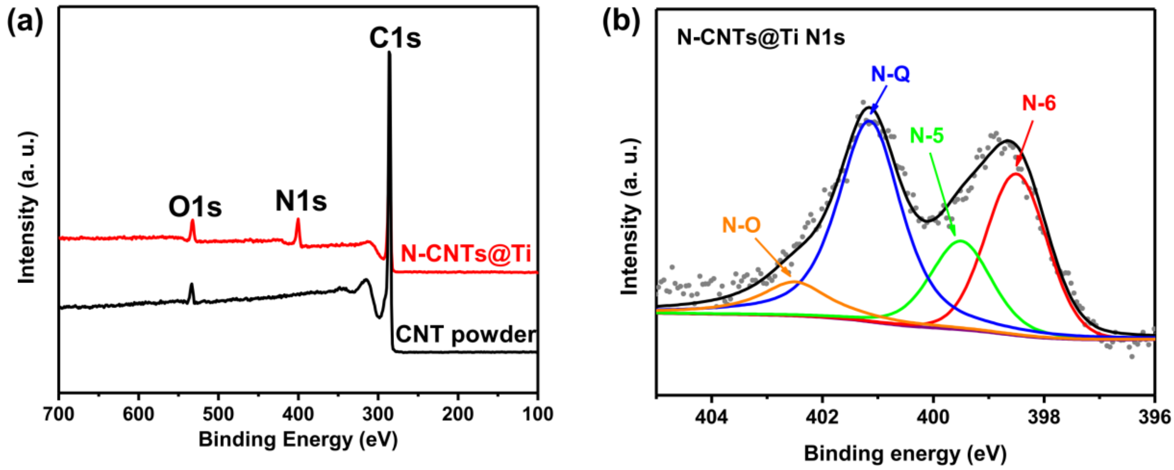

Figure S5. (a) XPS spectra of N-CNTs@Ti composite fiber and commercial CNT powder. (b) The high-resolution XPS spectrum of N 1s for N-CNTs@Ti, exhibiting four different doping categories of nitrogen atoms.

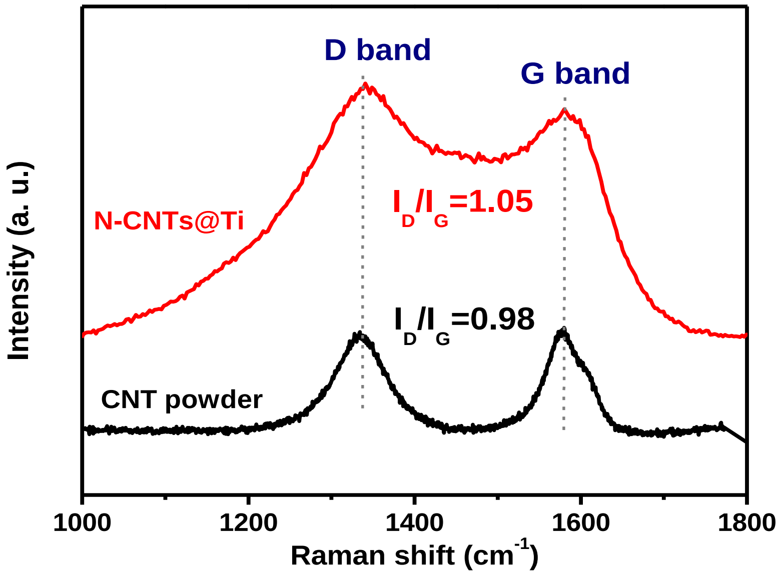

Figure S6. Raman spectra of N-CNTs@Ti and commercial CNT powder.

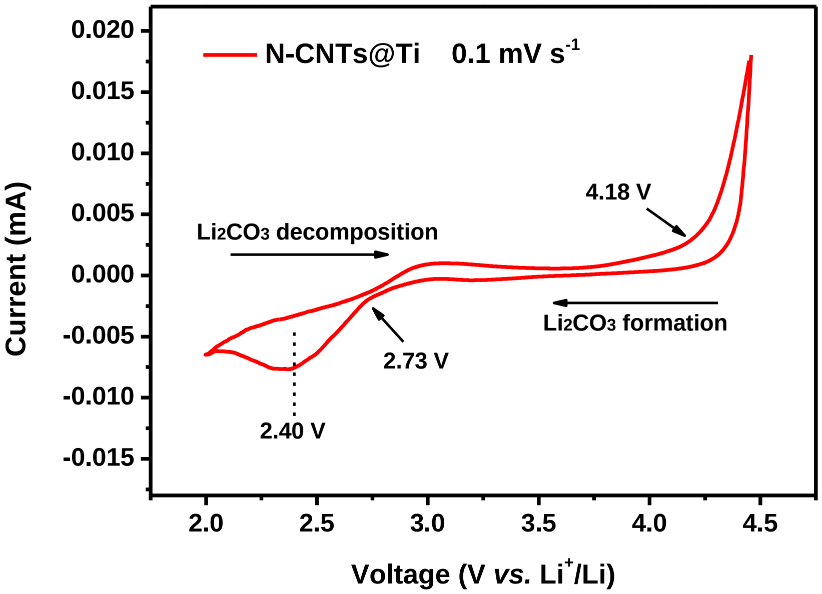

Figure S7. CV curves of the Li-CO_2 cell with a N-CNTs@Ti cathode under CO_2 at a scan rate of 0.1 mV s^{-1} over the voltage window of 2-4.5 V.

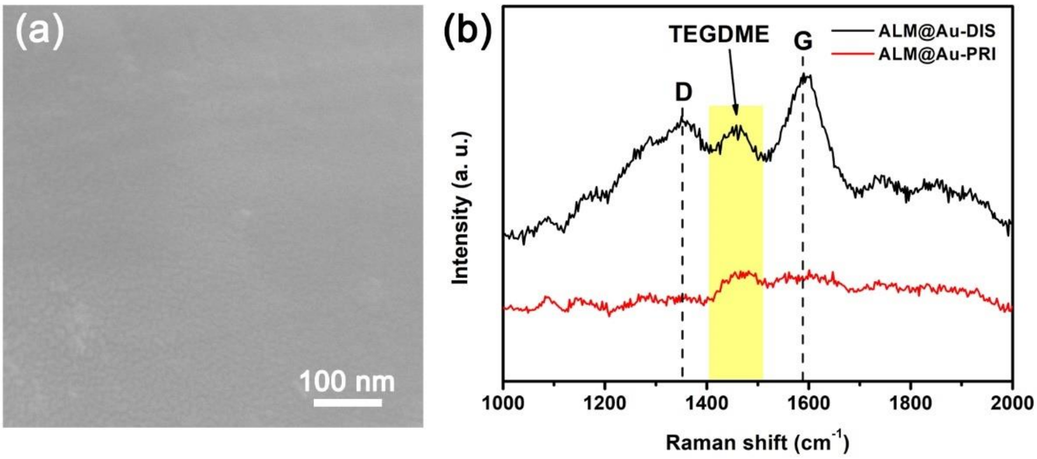

Figure S8. (a) The SEM image of Al mesh coated with Au nanoparticles (ALM@Au) as the none carbon-containing Li-CO_2 battery cathode for surface enhanced Raman spectroscopy (SERS) test. (b) Raman spectra collected on the gold cathode before (red line) and after (black line) discharging at 10 μA in CO_2 atmosphere.

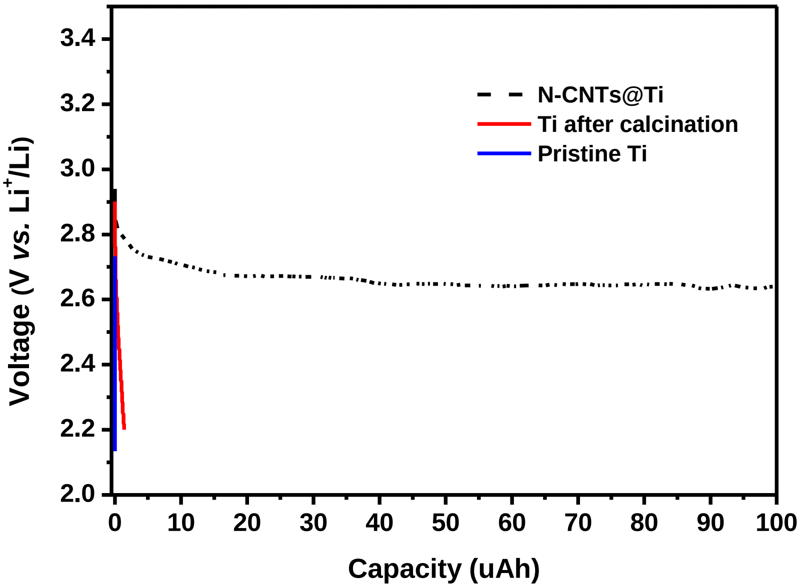

Figure S9. Galvanostatic discharge profiles of N-CNTs@Ti, pristine Ti wire and Ti wire after the same calcination process without carbon resources and catalyst precursors within the preliminary 100 μAh under CO_2 atmosphere.

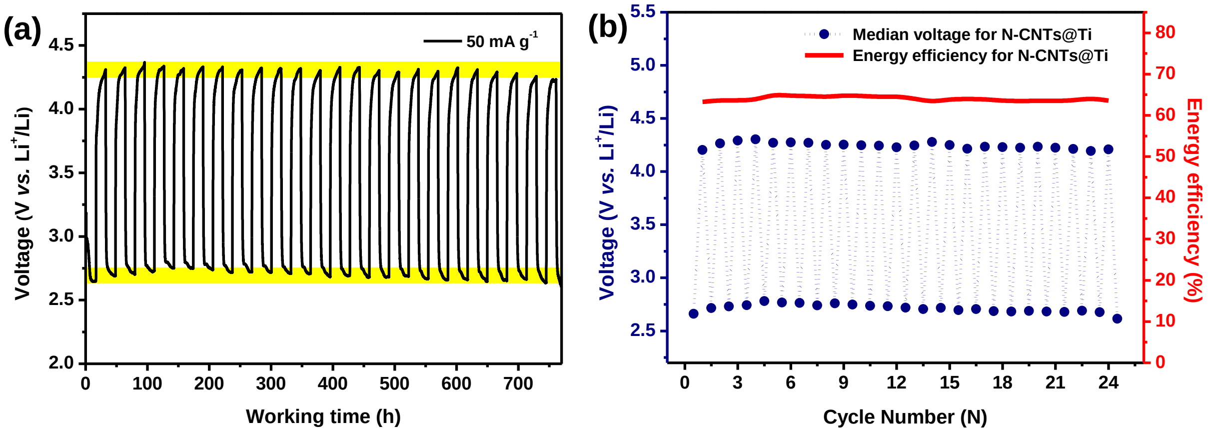

Figure S10. (a) Voltage-time curve of the Li-CO_2 battery with N-CNTs@Ti fibers as the working electrode at a current density of 50 mA g^{-1} and curtailing capacity of 1000 mAh g^{-1}. (b) Median voltages of discharge/charge plateaus with corresponding energy efficiencies inside of the Li-CO_2 cell at different cycles.

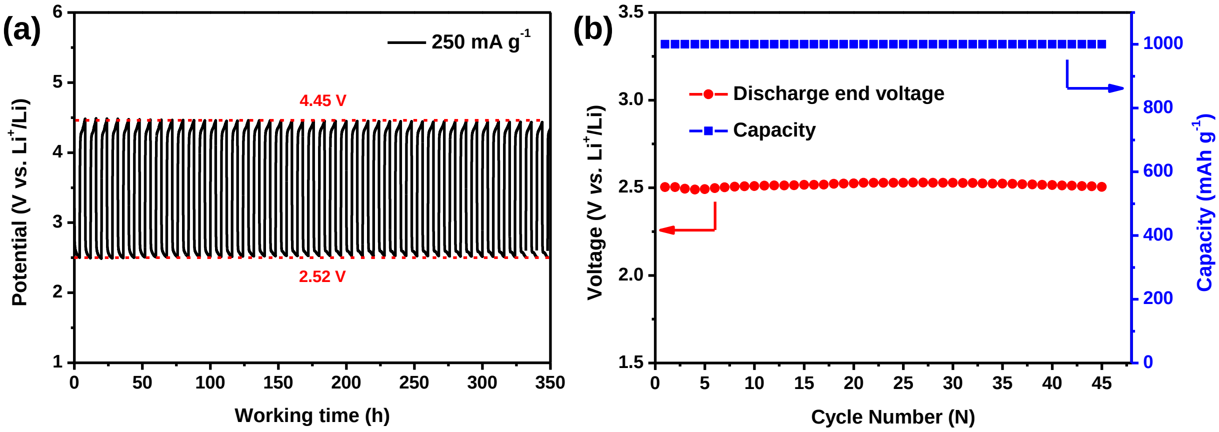

Figure S11. (a) Voltage-time curve of the Li-CO_2 battery with N-CNTs@Ti fibers as the working electrode at a current density of 250 mA g^{-1} and curtailing capacity of 1000 mAh g^{-1}. (b) The long-term cycling performance of the Li-CO_2 cell with a N-CNTs@Ti fibers cathode. The red line refers to the discharge end voltage while the blue line refers to curtailing capacity at every cycle. The cycling performance was tested with a current density of 250 mA g^{-1} and the discharge and charge capacities were limited to 1000 mAh g^{-1}.

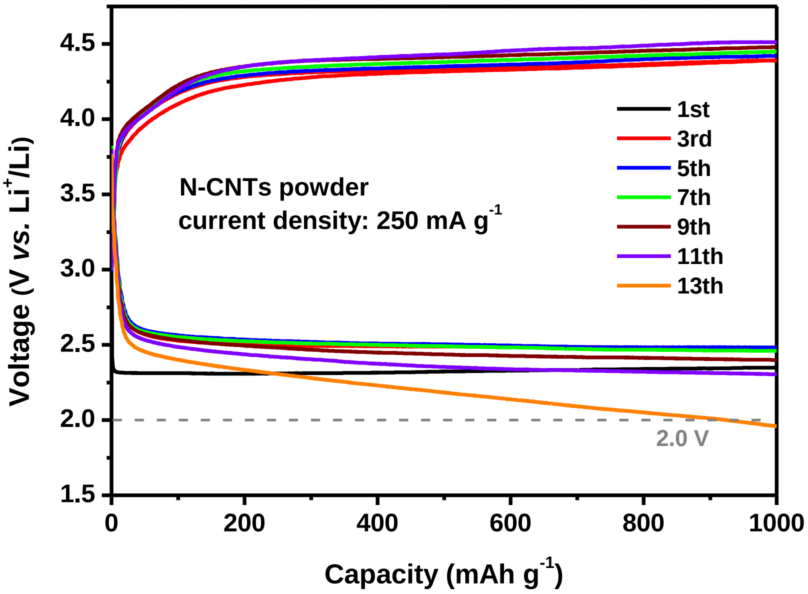

Figure S12. Galvanostatic discharge/charge profiles of commercial N-CNT powder cathode at the initial 13 cycles. The current density was set to 250 mA g^{-1} and the discharge/charge capacities were limited to 1000 mAh g^{-1}.

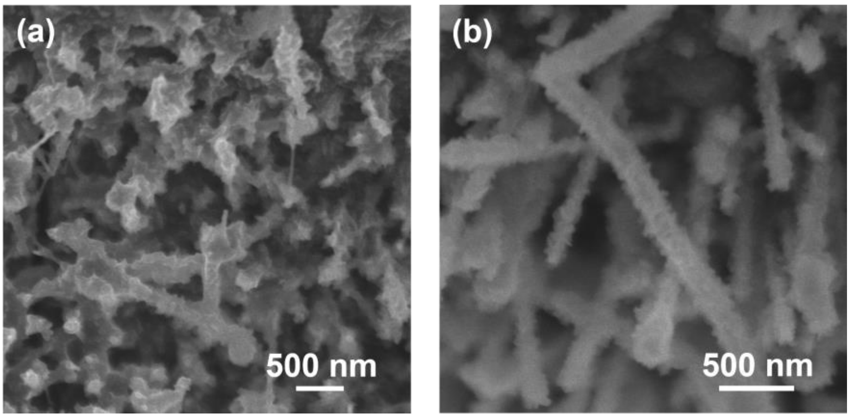

Figure S13. Typical SEM images of N-CNTs@Ti electrodes after the initial discharge process in CO_2 at different current densities of (a) 50 mA g^{-1} and (b) 250 mA g^{-1}, respectively, with a curtailing capacity of 1000 mAh g^{-1}.

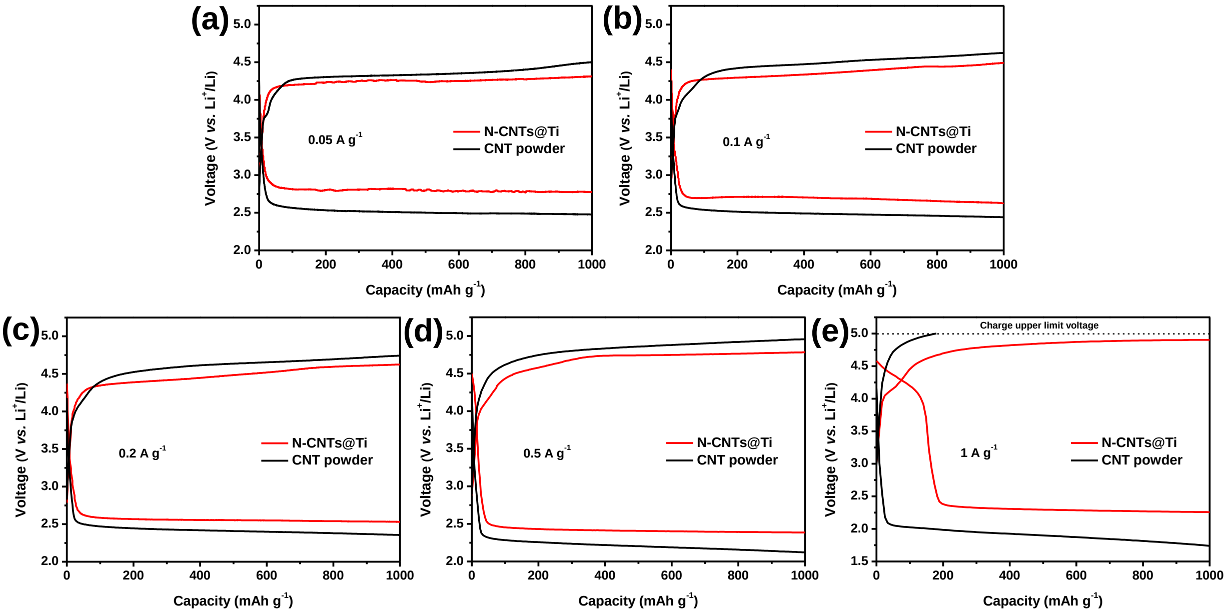

Figure S14. Comparison of galvanostatic discharge/charge profiles of the N-CNTs@Ti and commercial CNT powder cathodes at different current densities: (a) 0.05, (b) 0.1, (c) 0.2, (d) 0.5 and (e) 1 A g^{-1}. The capacity was limited to 1000 mAh g^{-1} during cycling.

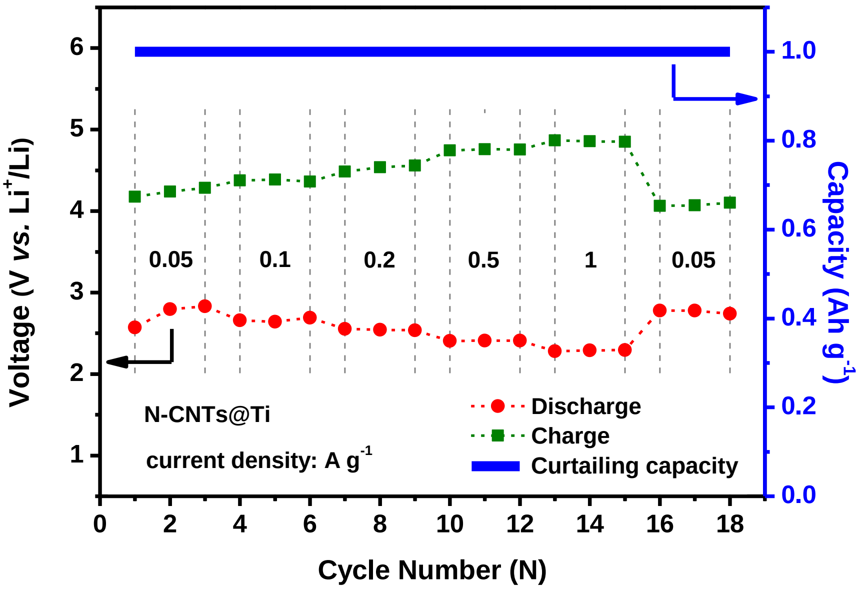

Figure S15. Rate performance of N-CNTs@Ti fiber at different current densities of 50, 100, 200, 500 and 1000 mA g^{-1} with the curtailing capacity of 1000 mAh g^{-1}, demonstrating the median voltages of discharge/charge processes.

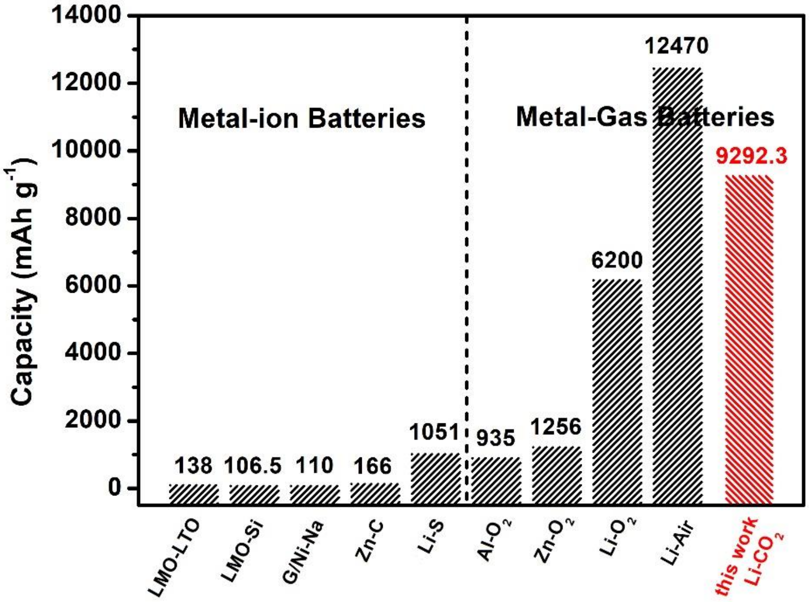

Figure S16. Comparison of specific capacity based on the weight of active materials between several typical kinds of fiber-shaped novel batteries, including the LMO-LTO battery,[S15] LMO-Si battery,[S16] G/Ni-Na battery,[S17] Zn-C battery,[S18] Li-S battery,[S19] Al-O_2 battery,[S20] Zn-O_2 battery,[S21] Li-O_2 battery[S22], ambient Li-air battery[S23] and Li-CO_2 battery in this work. The results were obtained from the data which these literatures provided, or by estimating based on the reported electrochemcial performances. Specifically, LMO and LTO represent $LiMn_2O_4$ and $Li_4Ti_5O_{12}$, respectively.

Table S1. Comparisons between several typical kinds of novel fiber-shaped batteries.

	Cathode	**Anode**	**State of electrolyte**	**Middle Discharge Voltage (V)**	**Capacity (mAh g^{-1})**
This work	N-CNTs@Ti fiber	Li wire	Liquid	2.67	9292.3
Li-ion battery[S1]	$LiMn_2O_4$@CNT fiber	$Li_4Ti_5O_{12}$@CNT fiber	Liquid	2.5	138
Li-ion battery[S2]	$LiMn_2O_4$@CNT fiber	CNT/Si/CNT fiber	Liquid	3.4	106.5
Na-ion battery[S3]	Carbon cloth@G@Ni sheet	Na sheet	Liquid	2.9	110
Zn-C battery[S4]	CNF@MnO_2 fiber	CNF@Zn powder fiber	Liquid	1.25	166
Li-S battery[S5]	S@CMK3@rGO@CNT fiber	Li wire	Liquid	2.1	1051
Al-Air battery[S6]	CNT@Ag NPs sheet	Al spring	GPE	1.25	935
Zn-Air battery[S7]	PTFE/AC@Fe/N/C sheet	Spiral Zn foil	GPE	0.9	1256
Li-Air battery[S8]	Carbon cloth@super P sheet	Li wire	GPE	2.65	6200
Li-Air battery[S9]	Aligned CNT array	Li wire	GPE	2.4	12470

Note: All of the above electrochemical data were obtained directly from the literatures or converted/evaluated based on the given electrochemical performances.

Table S2. Comparisons of electrochemical performances between previous Li-CO$_2$ batteries.

Cathode	**State of electrolyte**	**Mechanical Flexibility**	**Discharge Plateau (V)**	**Charge Plateau (V)**	**Capacity (mAh g^{-1})**	**Cycling Stability (N)**
N-CNTs@Ti fiber [this work]	Liquid	Y	2.83	4.2	9292.3	45
Super P powder[S10]	Liquid	N	2.7	4.2	1032	7
CNT powder[S11]	Liquid	N	2.7	4.3	8379	29
Graphene powder[S12]	Liquid	N	2.75	4.2	14722	20
RuO$_2$/LDO powder[S13]	Liquid	N	2.52	3.25	/	8
Carbon cloth@CoPPc film[S14]	Liquid	Y	2.8	4.0	13.6 mAh cm^{-2}	50
Mo$_2$C/CNT powder[S15]	Liquid	N	2.5	3.45	287.5	40
CNT cloth@Mo$_2$C NPs film[S16]	GPE	Y	2.68	3.39	3.415 mAh cm^{-2}	40
NiO-CNT powder[S17]	Liquid	N	2.7	4.1	9000	42
N-doped G@Cu NPs powder[S18]	Liquid	N	2.85	3.6	14864	50
Ru@Super P powder[S19]	Liquid	N	2.54	4.25	8229	70
Ir/CNFs powder[S20]	Liquid	N	2.76	4.14	21528	45
N-doped G@Ni NPs powder[S21]	Liquid	N	2.82	4.15	17625	101
CNT powder[S22]	GPE	N	2.7	4.35	8536	60
CNT powder[S23]	GPE at 55 □	Y	2.25	3.2	993.3 mAh	80

Note: All of the above electrochemical data were obtained directly from the literatures or converted/evaluated based on the given electrochemical performances.

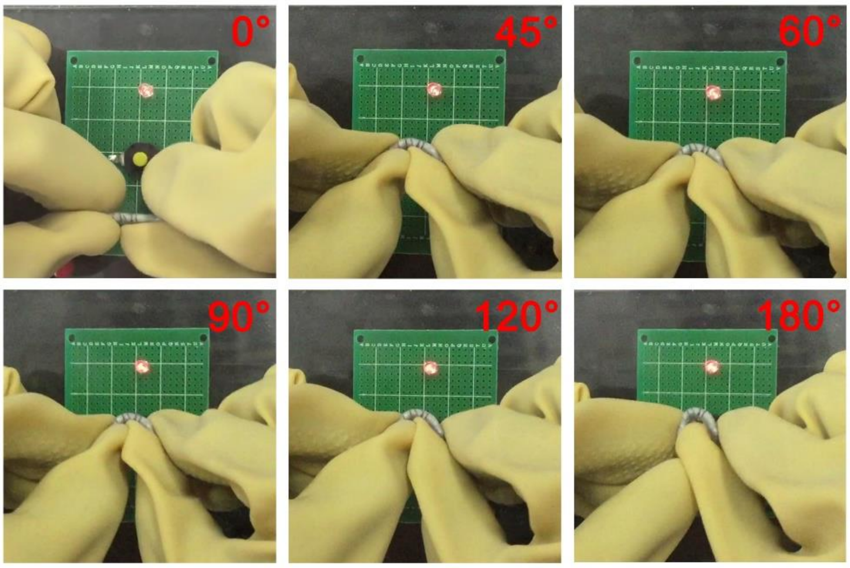

Figure S17. A red LED lit up by a 5 cm quasi-solid-state flexible fiber-shaped Li-CO_2 battery using N-CNTs@Ti as the cathode at different bending angles.

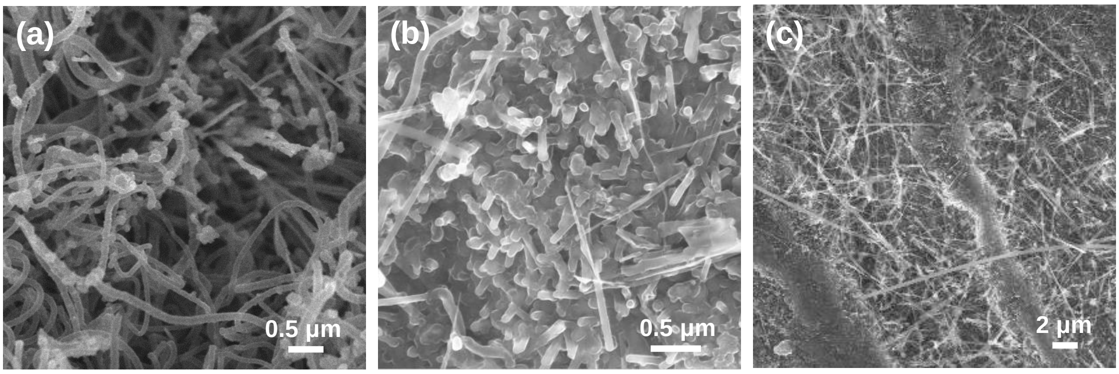

Figure S18. Typical SEM images of this N-CNTs@Ti hybrid fiber at different stages: (a) pristine, (b) discharged and (c) recharged.

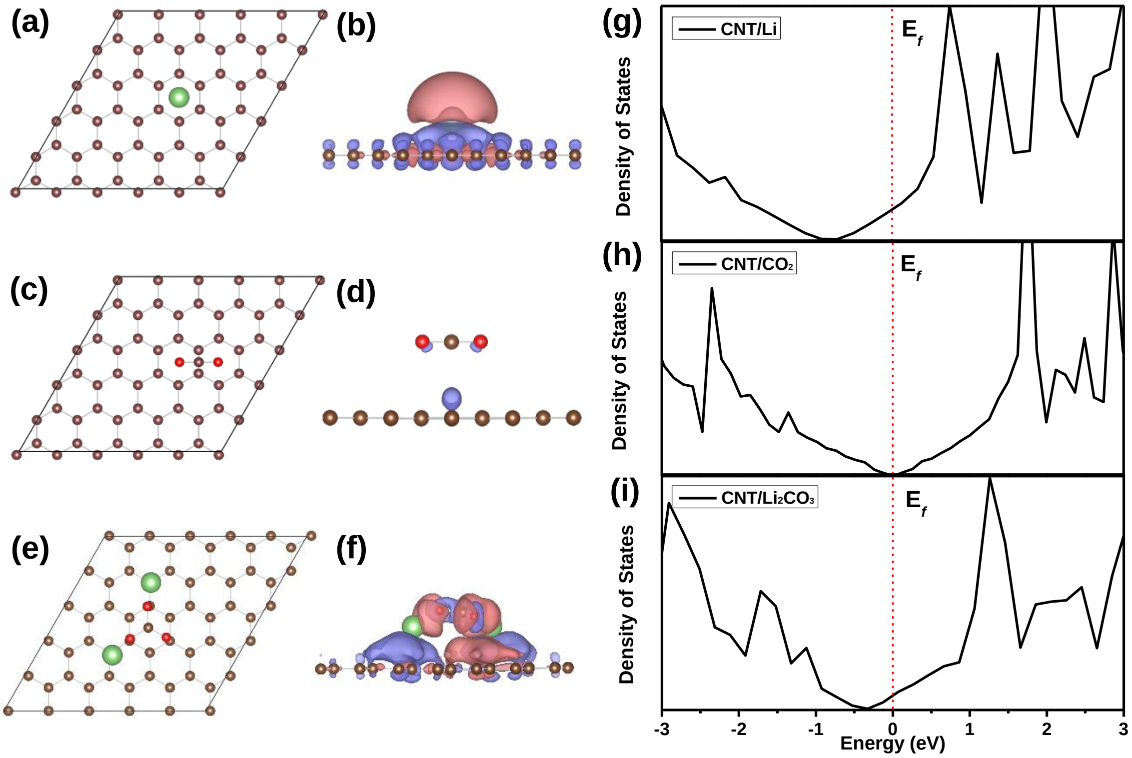

Figure S19. Top view of the optimized energetically most favorable structures of (a) Li, (c) CO_2 and (e) Li_2CO_3 adsorbed on pure CNT (002) surface. The brown, green and red balls represent C, Li and O, respectively. Charge density difference of (b) Li, (d) CO_2 and (f) Li_2CO_3 adsorbed on pure CNT (002) surface, respectively. The blue and pink regions represent the charge accumulation and charge loss, respectively. The isosurface value is set to be 0.001 e/Å^3. The electronic density of states (e-DOS) around the Fermi-level (E_f) of pure CNT after (g) Li, (h) CO_2 and (i) Li_2CO_3 was adsorbed on the surface.

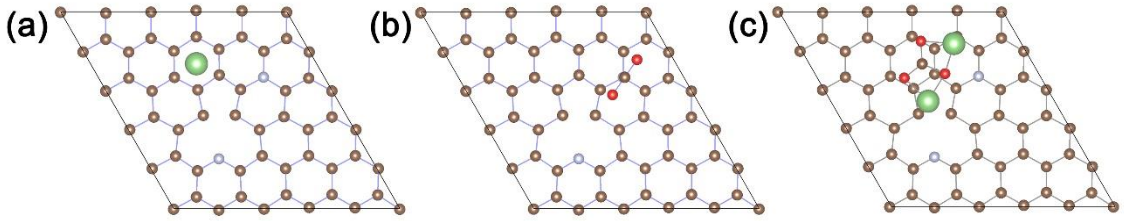

Figure S20. Top view of the optimized energetically most favorable structures of (a) Li, (b) CO_2 and (c) Li_2CO_3 adsorbed on N-Q site of pyridinic and graphitic N-doped CNT (002) surface. The brown, green and red balls represent C, Li and O, respectively.

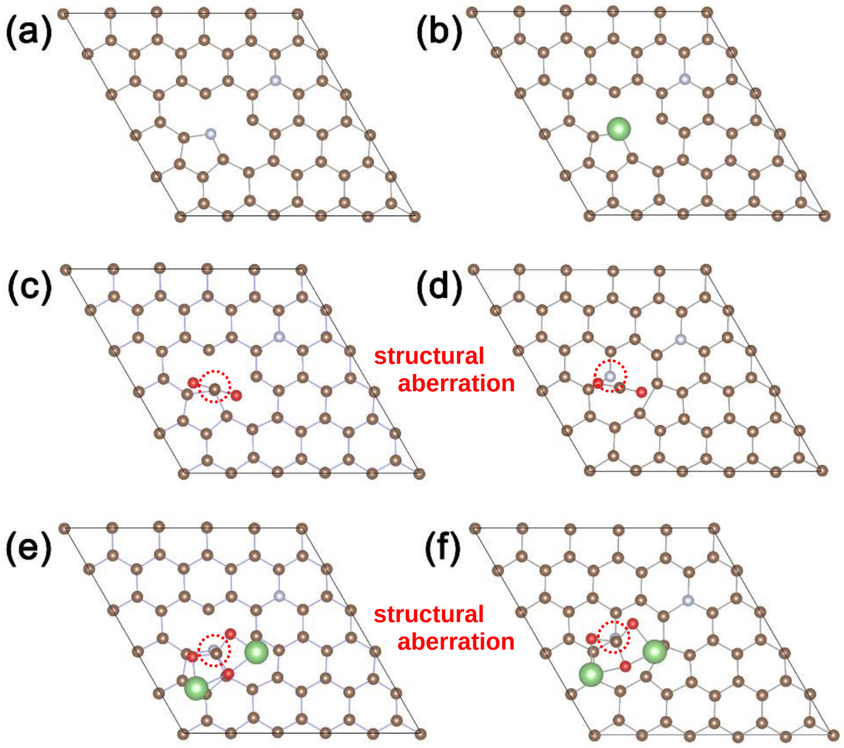

Figure S21. (a) Top view of pyrrolic and graphitic N-doped CNT (002) surface. (b) Top view of the optimized energetically most favorable structures of Li adsorbed on N-5 site. Top view of CO_2 adsorbed on N-5 site (c) before and (d) after energy optimization. Top view of Li_2CO_3 adsorbed on N-5 site (c) before and (d) after energy optimization. The brown, green and red balls represent C, Li and O, respectively.

References

[1] J. Ren, Y. Zhang, W. Bai, X. Chen, Z. Zhang, X. Fang, W. Weng, Y. Wang, H. Peng, *Angew. Chem. Int. Ed.* **2014**, *126*, 7998.

[2] W. Weng, Q. Sun, Y. Zhang, H. Lin, J. Ren, X. Lu, M. Wang, H. Peng, *Nano Lett.* **2014**, *14*, 3432.

[3] Y. Zhu, S. Yuan, D. Bao, Y. Yin, H. Zhong, X. Zhang, J. Yan, Q. Jiang, *Adv. Mater.* **2017**, *29*, 1603719.

[4] X. Yu, Y. Fu, X. Cai, H. Kafafy, H. Wu, M. Peng, S. Hou, Z. Lv, S. Ye, D. Zou, *Nano Energy* **2013**, *2*, 1242.

[5] X. Fang, W. Weng, J. Ren, H. Peng, *Adv. Mater.* **2016**, *28*, 491.

[6] Y. Xu, Y. Zhao, J. Ren, Y. Zhang, H. Peng, *Angew. Chem. Int. Ed.* **2016**, *55*, 7979.

[7] J. Park, M. Park, G. Nam, J. Lee, J. Cho, *Adv. Mater.* **2015**, *27*, 1396.

[8] T. Liu, Q. Liu, J. Xu, X. Zhang, *Small* **2016**, *12*, 3101.

[9] Y. Zhang, L. Wang, Z. Guo, Y. Xu, Y. Wang, H. Peng, *Angew. Chem. Int. Ed.* **2016**, *55*, 4487.

[10] Y. Liu, R. Wang, Y. Lyu, H. Li, L. Chen, *Energy Environ. Sci.* **2014**, *7*, 677.

[11] X. Zhang, Q. Zhang, Z. Zhang, Y. Chen, Z. Xie, J. Wei, Z. Zhou, *Chem. Commun.* **2015**, *51*, 14636.

[12] Z. Zhang, Q. Zhang, Y. Chen, J. Bao, X. Zhou, Z. Xie, J. Wei, Z. Zhou, *Angew. Chem. Int. Ed.* **2015**, *54*, 6550.

[13] S. Xu, Z. Ren, X. Liu, X. Liang, K. Wang, J. Chen, *Energy Storage Mater.* **2018**, *15*, 291.

[14] J. Chen, K. Zou, P. Ding, J. Deng, C. Zha, Y. Hu, X. Zhao, J. Wu, J. Fan, Y. Li, *Adv. Mater.* **2018**, *30*, 1805484.

[15] Y. Hou, J. Wang, L. Liu, Y. Liu, S. Chou, D. Shi, H. Liu, Y. Wu, W. Zhang, J. Chen, *Adv. Funct. Mater.* **2017**, *27*, 1700564.

[16] J. Zhou, X. Li, C. Yang, Y. Li, K. Guo, J. Cheng, D. Yuan, C. Song, J. Lu, B. Wang, *Adv.*

Mater. **2018**, *30*, 1804439.

[17] X. Zhang, C. Wang, H. Li, X. Wang, Y. Chen, Z. Xie, Z. Zhou, *J. Mater. Chem. A* **2018**, *6*, 2792.

[18] Z. Zhang, Z. Zhang, P. Liu, Y. Xie, K. Cao, Z. Zhou, *J. Mater. Chem. A* **2018**, *6*, 3218.

[19] S. Yang, Y. Qiao, P. He, Y. Liu, Z. Cheng, J. Zhu, H. Zhou*, Energy Environ. Sci.* **2017**, *10*, 972.

[20] C. Wang, Q. Zhang, X. Zhang, X. Wang, Z. Xie, Z. Zhou, *Small* **2018**, *14*, 1800641.

[21] Z. Zhang, X. Wang, X. Zhang, Z. Xie, Y. Chen, L. Ma, Z. Peng, Z. Zhou, *Adv. Sci.* **2017**, *5*, 1700567.

[22] C. Li, Z. Guo, B. Yang, Y. Liu, Y. Wang, Y. Xia, *Angew. Chem. Int. Ed.* **2017**, *129*, 9254.

[23] X. Hu, Z. Li, J. Chen, *Angew. Chem. Int. Ed.* **2017**, *56*, 5785.